Fermi-Surface Reconstruction and Complex Phase Equilibria in $CaFe_2As_2$

K. Gofryk,[1*] B. Saparov,[1] T. Durakiewicz,[2] A. Chikina,[3,4] S. Danzenbächer,[4] D. V. Vyalikh,[3,4] M. J. Graf,[2] and A. S. Sefat[1]

[1]*Oak Ridge National Laboratory, Oak Ridge, Tennessee 37831, USA*
[2]*Los Alamos National Laboratory, Los Alamos, New Mexico 87545, USA*
[3]*Department of Physics, St. Petersburg State University, St. Petersburg 198504, Russia*
[4]*Institute of Solid State Physics, Dresden University of Technology, Zellescher Weg 16, D-01062 Dresden, Germany*

(Received 19 September 2013; revised manuscript received 23 January 2014; published 7 May 2014)

Fermi-surface topology governs the relationship between magnetism and superconductivity in iron-based materials. Using low-temperature transport, angle-resolved photoemission, and x-ray diffraction, we show unambiguous evidence of large Fermi-surface reconstruction in $CaFe_2As_2$ at magnetic spin-density-wave and nonmagnetic collapsed-tetragonal (cT) transitions. For the cT transition, the change in the Fermi-surface topology has a different character with no contribution from the hole part of the Fermi surface. In addition, the results suggest that the pressure effect in $CaFe_2As_2$ is mainly leading to a rigid-band-like change of the valence electronic structure. We discuss these results and their implications for magnetism and superconductivity in this material.

DOI: 10.1103/PhysRevLett.112.186401 PACS numbers: 71.27.+a, 72.15.Qm, 74.70.Tx, 74.90.+n

$CaFe_2As_2$ has a special position among the $ThCr_2Si_2$-type AFe_2As_2 (A = Ba, Sr, Ca) superconducting phases [1–3] due to a complex relationship between magnetism, superconductivity, and lattice instabilities (see Refs. [4–6]). The way $CaFe_2As_2$ is typically grown under ambient pressure makes it crystallize in the tetragonal (T) crystal structure at room temperature, which then undergoes a simultaneous spin-density-wave (SDW) and orthorhombic (O) transition at ~170 K [7,8]. Application of a small amount of pressure or introducing chemical dopants rapidly suppresses the transition in $CaFe_2As_2$, and superconductivity is observed at low temperatures [9]. At higher pressures, there is a transition to the nonmagnetic collapsed-T (cT) phase [10], where a significant reduction of the c-axis length is observed (see Fig. 1). $CaFe_2As_2$ is also very sensitive to nonhydrostacity, and the presence of a superconducting state strongly depends on the way the pressure is transmitted to the sample [11–13]. Therefore, the interplay of the Fermi-surface nesting and strong spin-lattice coupling is a key parameter for understanding the origin of magnetism and superconductivity in $CaFe_2As_2$ and other Fe-based materials in general.

The band structure calculations suggest that $CaFe_2As_2$ undergoes a large Fermi-surface reconstruction at the SDW/structural transitions. In the high-temperature T phase, the Fermi surface has a strongly two-dimensional (2D) character with two warped electron cylinders at the corners of the Brillouin zone (M) and two hole cylinders at the zone center (Γ) [17–19]. During transformation to the magnetic O phase, the electron pocket remains quasi 2D, although the hole cylinder forms a three-dimensional oval [20,21]. Recent angle-resolved photoemission spectroscopy (ARPES) and quantum oscillation measurements indeed show a dramatic change of the Fermi-surface topology in $CaFe_2As_2$ at 170 K [22–26]. In the cT phase, the theoretical calculations also predict a major topological change of the Fermi surface: the two electron pockets at the M point transform into one cylinder, whereas the hole pockets at Γ disappear [21,27–29]. In these contexts, it is important to understand the mechanism of the Fermi-surface renormalization that influences the electronic properties of the competing phases in $CaFe_2As_2$ and its relationship to magnetism and superconductivity, especially the cT phase. The nature of the cT phase, however, is still not well accounted and understood, and ARPES results are missing.

Here we use extensive transport, angle-resolved photoemission, and x-ray diffraction measurements to study the Fermi-surface reconstruction and complex phase equilibria in $CaFe_2As_2$ crystals at different crystallographic structures. By proper annealing procedure [12], we are able to synthesize and study samples of $CaFe_2As_2$ that can be placed at specific parts of the phase diagram (see the red solid arrows in Fig. 1). Therefore, we can access directly the cT phase and also track changes in the electronic properties similar to $CaFe_2As_2$ under pressure. We show that the Fermi surface of $CaFe_2As_2$ experiences a large reconstruction at the SDW transition, especially at the hole part of the respective Fermi surfaces. The change in the Fermi-surface topology has a different character when the sample transforms to the nonmagnetic cT phase, where we do not observe any significant contribution from the hole sheets of the Fermi surface. The pressure effect can be linked to the renormalization of the band structure governed by the strength of interband interactions, as identified by direct measurement of the Fermi-surface renormalization with ARPES, and modeling.

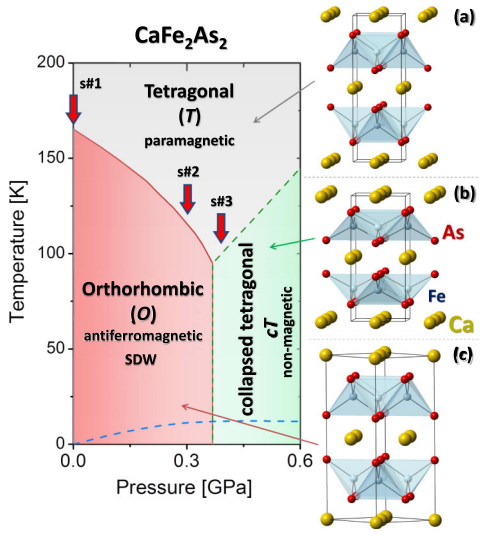

FIG. 1 (color online). A putative phase diagram of $CaFe_2As_2$. The data are adapted from Refs. [9,14–16]. The blue dashed line marks superconductivity in $CaFe_2As_2$ observed under a non-hydrostatic pressure condition [14]. On the right side, the crystal structures of (a) T (s.g. $I4/mmm$), (b) cT, and (c) O (s.g. $Fmmm$) phases are presented. The structures are drawn with modified parameters in order to emphasize the differences between the three phases. The thick solid red arrows mark the transition temperatures of samples studied in this work (see text).

Crystals of $CaFe_2As_2$ were grown out of FeAs flux with the typical size of about $2 \times 2 \times 0.1$ mm^3. By proper thermal annealing, $CaFe_2As_2$ can be tuned to a low-temperature antiferromagnetic O or a nonmagnetic cT state, all at ambient pressure, although a bulk superconducting state in never observed [12]. We study three single crystals of $CaFe_2As_2$ extracted from the same batch [30]. The first sample ($s1$) has been annealed at 350 °C for 5 days and shows antiferromagnetic ordering below $T_N \simeq 168$ K. The second sample ($s2$) was annealed at 700°C for 1 day and exhibits $T_N \simeq 116$ K. The third sample ($s3$) is as-grown $CaFe_2As_2$ crystal showing transition to the nonmagnetic cT phase at $T_{tr} \simeq 95$ K (see Fig. 1). The transport properties were measured using a Quantum Design PPMS-14 setup. The low-temperature diffraction experiments were carried out using a PANalytical X'Pert PRO MPD x-ray diffractometer with Cu-$K_{\alpha 1}$ radiation. ARPES measurements were performed at Swiss light source on the SIS-X09LA beam line. We used 82-eV photons, with an instrumental resolution of ~15 meV and base vacuum better than 6×10^{-11} mbar.

The electronic transport, especially Hall and Seebeck effects, is an effective probe of the Fermi-surface volume and density of states in the vicinity of the Fermi level. Recently, the transport measurements have been used successfully to reveal details of the Fermi-surface topology in heavy fermions, cuprates, and Fe-based superconductors [31–36]. Figure 2 shows the temperature dependence of the electrical resistivity [$\rho(T)$], Hall [$R_H(T)$], and Seebeck [$S(T)$] coefficients of $CaFe_2As_2$ crystals. It is worth noting that all of the transport properties obtained for $s1$ show similar behaviors to the ones reported for Sn-flux grown $CaFe_2As_2$ with $T_N \simeq 170$ K (see Refs. [8,37]). The increase of $\rho(T)$ below $T_N = 168$ K is consistent with the presence of the SDW state in $CaFe_2As_2$ and can be understood by the Suezaki and Mori model [38]. At the transition temperature, both R_H and S change sign and become positive. In addition, the discontinuous nature of the transition and the presence of narrow hysteresis of the order of 2 K (see the Supplemental Material [39] for more details) are consistent with the first-order character of the phase transition in this sample. The behavior of the Hall and Seebeck effects is characteristic of metals with electronic transport governed by electron and hole bands, in agreement with the electronic structure calculated for the T phase of $CaFe_2As_2$ [21,27–29]. Below the transition, the electronic structure is strongly reconstructed and shows a significant contribution from the hole type of the Fermi sheets. At low temperatures, the Hall and Seebeck coefficient changes signs to negative, most probably due to higher mobility of the electron carriers. A single-band model provides an estimate for the concentration of free electrons n_H of 1.2×10^{23} cm^{-3} and 6.8×10^{20} cm^{-3} at 250 K and 5 K, respectively. This should be considered as the upper limit of the actual carrier concentrations. However, besides this crude approximation, the drop of n_H below T_N is consistent with the Fermi-surface gapping scenario. All of these results support recent band structure calculations [21,29] and are consistent with ARPES and quantum oscillation measurements of $s1$, which is typically studied phase [22–26].

The overall transport properties of $s2$ ($T_N \simeq 116$ K) are similar to those of $s1$ (see Fig. 2). The electrical resistivity shows a pronounced maximum below the magnetic and structural transition. Similarly, as shown by Hall and Seebeck measurements, below the transition, R_H and S start to rise, but their overall change is not as rapid as observed in $s1$ [39]. In addition, the width of the transitions is much wider as well as a range of the hysteretic behavior. This could point to a similar but significantly weaker change of the electronic structure in this material at the transition. We attribute this behavior to the large range of the phase coexistence in this sample [39], which creates a significant difficulty in studying the effect of the Fermi-surface reconstruction of the hole pockets at the transition region, as it was possible in $s1$. At low temperatures, however, the Hall and Seebeck data agree well, indicating similar physics involved.

A remarkably different situation is observed for the $CaFe_2As_2$ $s3$ phase. As shown in Fig. 2, all of the transport coefficients experience a rapid change at the transition to the cT phase, accompanied by a small thermal hysteresis, both being consistent with the first-order nature of the transition [39]. This change, however, has different character than previously observed in the $s1$ and $s2$ samples. In

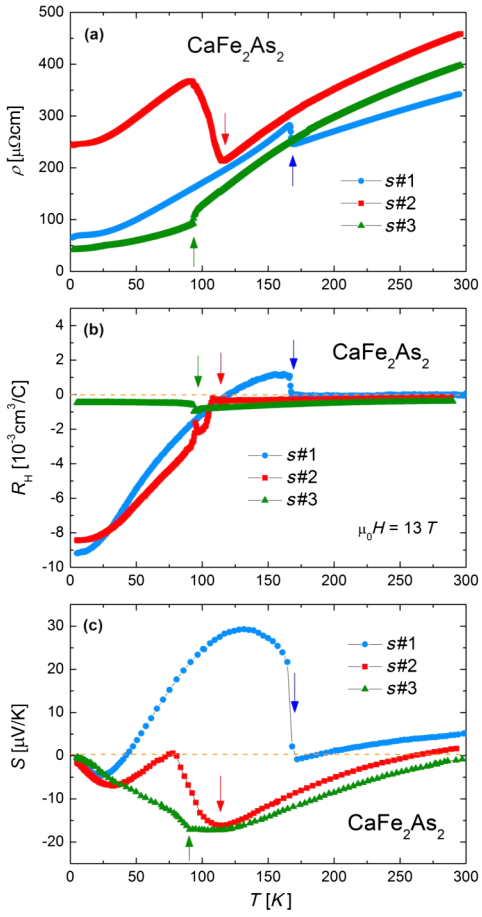

FIG. 2 (color online). The temperature dependencies of the electrical resistivity (a), Hall effect (b), and Seebeck coefficient (c) of $CaFe_2As_2$ single crystals. All of the curves were measured on cooling the samples. The arrows mark the antiferromagnetic ($s1$ and $s2$) and cT ($s3$) phase transitions (see text).

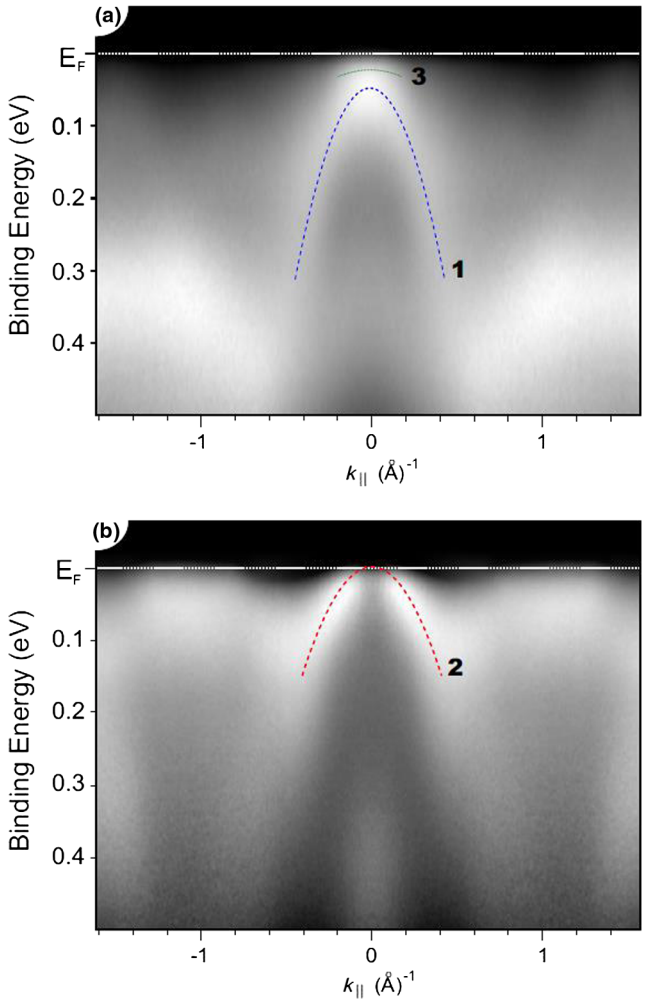

FIG. 3 (color online). Band renormalization upon the T/cT transition measured by ARPES. (a) and (b) The $\Gamma - X$ direction in the Brillouin zone mapped for the cT and T samples, respectively. A clear shift in binding energy of the main holelike band in the zone center may be noted. See the text and [39] for more details.

the T phase, both R_H and S show a similar temperature dependence to the previously discussed samples. At the cT transition, the electrical resistivity drops, most probably due to an increase of the carrier concentration (see below). In contrast to the situation described for $s1$ and $s2$, for $s3$ and below T_{tr}, the Hall effect and thermoelectric power do not change sign, but instead, their magnitude decreases. This indicates that the Fermi-surface reconstruction to the cT phase does not create a significant, if any, holelike topology as has been observed for magnetically ordered $CaFe_2As_2$. Furthermore, the transition to the cT phase increases the electronlike Fermi-surface volume in this material, as shown by the Hall effect. The electron carrier concentration increases from 6.8×10^{21} cm^{-3} just above the transition to 1.1×10^{22} cm^{-3} below T_{tr}. It has been predicted that the electronic structure of the T and cT phases are surprisingly similar despite the large c-axis reduction [29]. Furthermore, it was concluded that the cT phase has a lower energy compared to the T phase, so most of the bands are just shifted to lower energy in the cT phase.

The results of angle-resolved photoemission study, shown in Fig. 3, clearly show that indeed a band shift toward higher binding energies upon the T/cT transition is the dominant band structure effect upon entering the collapsed phase. Specifically, the bands just above the Fermi level in the T phase move below the Fermi level (E_F) in cT phase, altogether leading to disappearance of the hole pocket at the center of Brillouin zone [28]. Moreover, since only one electronlike band crosses the Fermi level along $\Gamma - M$ direction, the total density of states at E_F is reduced as compared to the T phase [27–29]. Besides the band shift, we also observe a change in effective mass, where effective masses for bands 1, 2, and 3 in Fig. 3 are estimated as—2.8,—4.1, and approximately—15–20 m_e, respectively. This would correspond to a mass enhancement factor of about four to five upon transition from T to cT phase, assuming the band closest to the Fermi level for

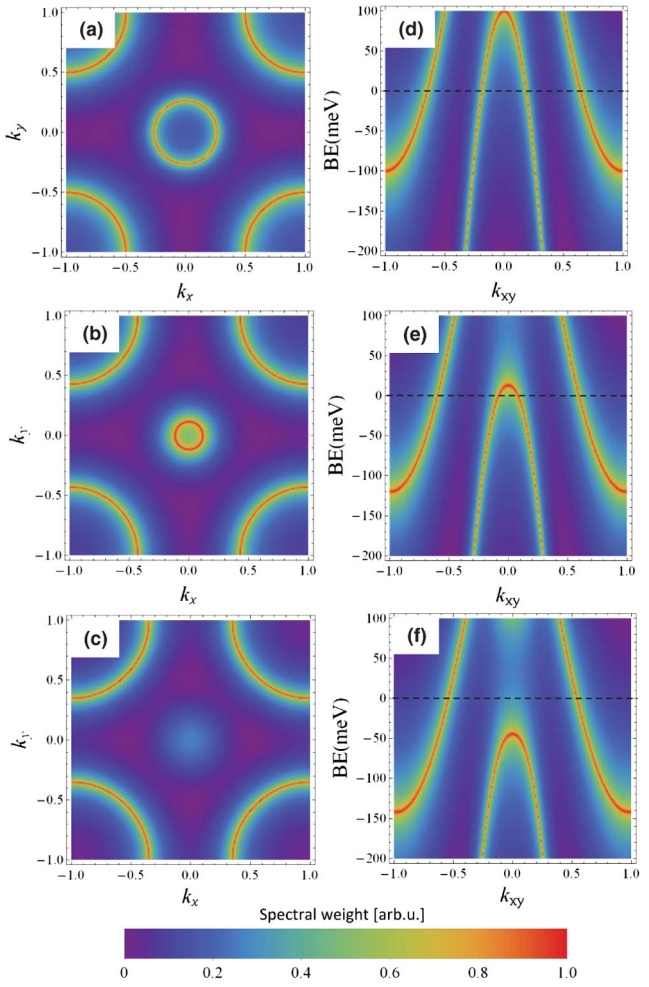

FIG. 4 (color online). Modeling the band renormalization sequence. (a—c) The $k_x - k_y$ cuts of the Fermi surface. (d—f) The corresponding $k_{xy} - \omega$ cuts of the near-Fermi-level region of the electronic band structure (k, momentum in reciprocal space). Interband coupling strength is increased from 0 in (a) and (d) to a maximum value in (c) and (f). See the text and [39] for more details.

mass renormalization considerations. It should be noted here that while bands 1 and 2 are relatively well pronounced, band 3 shows much less spectral intensity. Also, the structure around band 2 may contain another holelike band of similar effective mass, which was not resolved here. These points do not change our central conclusions of (i) band shift and (ii) mass enhancement upon transition.

The disappearance of the hole pocket at the Γ point has a dramatic consequence for magnetism and superconductivity since interplay of the Fermi-surface nesting and strong spin-lattice coupling has been proposed to control those phenomena in Fe-based superconductors [17–19]. ARPES measurements confirm the transport results and show a distinct evolution of the band structure renormalization at the T to cT transition in $s3$, observed from the Z point in the zone center toward the Γ point belonging to the next body-centered tetragonal zone. Here, a shift of the band structure toward higher binding energies is observed as a dominant effect at the transition. The observed shift is momentum dependent, spanning a range from about 50 meV for the holelike band in the zone center to about 100 meV for the electronlike band at the Γ point. Shift of the holelike band below the Fermi level is accompanied by (i) destruction of the centrally located small holelike Fermi surface and (ii) an increase an effective mass, as indicated by the flatlike parts of renormalized spectral weight appearing at the top of the band.

We propose that the above discussed properties can be linked to the renormalization of the electronic structure driven by the evolution of electronic interband coupling constants. We approach this model from the point of view of the rigid but momentum-dependent band shift that can be visualized by application of a single parameter, namely the interband scattering strength or coupling constant λ [40,41]. The results of this simulation are in very good agreement with experimental momentum-resolved electronic structure renormalization through the transition obtained from ARPES and are shown in Fig. 4. Here we start with a high-temperature band structure, simplified after [42,43], shown in Figs. 4(a) and 4(d). This structure is used in the model as the bare-band or nonrenormalized structure, with $\lambda = 0$. Upon increasing pressure or equivalently the interband coupling strength λ, we observe the central holelike band to be shifted below the Fermi level, while its effective mass increases by about a factor of 2, in agreement with transport measurements of T and cT phases, and ARPES results. This observation provides a useful link between the transport and electronic properties and is verified by photoemission experiments.

In summary, we have investigated the electronic properties of $CaFe_2As_2$ crystals with different magnetic or crystallographic structures. We show that the Fermi-surface topology, especially the hole part of the Fermi surface, experiences a large reconstruction at the SDW/structural transition. For the crystal that shows the transition to the nonmagnetic cT phase, the reconstruction of the Fermi surface is different, and we do not observe a significant contribution from the hole part of the Fermi surface. Furthermore, our data, especially the combination of ARPES measurements and interband scattering model, together with the evolution of the Hall and Seebeck effect and magnitude of the cotangent of Hall angle (see [39]), suggest that the effect of pressure on change in the Fermi-surface topology results mainly in rigid-band shift to lower energy. These new results extend our understanding of this system beyond the recent band structure calculations [27–29] and form the basis of our proposed renormalized band structure model. The disappearance of the hole pockets in the cT phase prevents Fermi-surface nesting, which has been proposed to be a necessary ingredient for magnetism and spin-fluctuation-mediated superconductivity in iron-base materials [17–19]. This

fully explains a lack of magnetism and bulk superconductivity in the cT phase of $CaFe_2As_2$.

Work at ORNL was supported by the U.S. Department of Energy, Basic Energy Sciences, Materials Sciences and Engineering Division. Department of Energy, Office of Basic Energy Sciences, and LANL LDRD programs supported work at LANL. A. C. and D. V. V. acknowledge the DFG grants GRK1621 and LA655/12-1.

Note added in proof.—During preparation of this manuscript, we became aware of Ref. [44], where ARPES measurements were used to determine electronic properties of $CaFe_2As_2$ in cT phase. The obtained change in Fermi surface topology at cT transition in Ref. [44] is in good agreement with results presented here.

*Present address: Idaho National Laboratory, Idaho Falls, Idaho 83415, USA

[1] M. Rotter, M. Tegel, and D. Johrendt, Phys. Rev. Lett. **101**, 107006 (2008).
[2] A. S. Sefat, R. Jin, M. A. McGuire, B. C. Sales, D. J. Singh, and D. Mandrus, Phys. Rev. Lett. **101**, 117004 (2008).
[3] A. Leithe-Jasper, W. Schnelle, C. Geibel, and H. Rosner, Phys. Rev. Lett. **101**, 207004 (2008).
[4] A. I. Goldman, D. Argyriou, B. Ouladdiaf, T. Chatterji, A. Kreyssig, S. Nandi, N. Ni, S. Bud'ko, P. Canfield, and R. McQueeney, Phys. Rev. B **78**, 100506(R) (2008).
[5] K. Prokeš, A. Kreyssig, B. Ouladdiaf, D. K. Pratt, N. Ni, S. L. Bud'ko, P. C. Canfield, R. J. McQueeney, D. N. Argyriou, and A. I. Goldman, Phys. Rev. B **81**, 180506 (R) (2010).
[6] S. K. Mishra *et al.*, arXiv:1304.0595.
[7] N. Ni, S. L. Bud'ko, A. Kreyssig, S. Nandi, G. E. Rustan, A. I. Goldman, S. Gupta, J. D. Corbett, A. Kracher, and P. C. Canfield, Phys. Rev. B **78**, 014507 (2008).
[8] F. Ronning, T. Klimczuk, E. D. Bauer, H. Volz, and J. D. Thompson, J. Phys. Condens. Matter **20**, 322201 (2008).
[9] P. C. Canfield, S. L. Bud'ko, N. Ni, A. Kreyssig, A. I. Goldman, R. J. McQueeney, M. S. Torikachvili, D. N. Argyriou, G. Luke, and W. Yu, Physica C (Amsterdam) **469**, 404 (2009).
[10] J. H. Soh *et al.*, Phys. Rev. Lett. **111**, 227002 (2013).
[11] W. Yu, A. Aczel, T. Williams, S. Bud'ko, N. Ni, P. Canfield, and G. Luke, Phys. Rev. B **79**, 020511(R) (2009).
[12] S. Ran *et al.*, Phys. Rev. B **83**, 144517 (2011).
[13] A. S. Sefat, Rep. Prog. Phys. **74**, 124502 (2011).
[14] M. S. Torikachvili, S. L. Budko, N. Ni, and P. C. Canfield, Phys. Rev. Lett. **101**, 057006 (2008).
[15] A. I. Goldman *et al.*, Phys. Rev. B **79**, 024513 (2009).
[16] H. Lee, E. Park, T. Park, V. Sidorov, F. Ronning, E. Bauer, and J. Thompson, Phys. Rev. B **80**, 024519 (2009).
[17] I. I. Mazin, D. J. Singh, M. D. Johannes, and M. H. Du, Phys. Rev. Lett. **101**, 057003 (2008).
[18] K. Seo, B. A. Bernevig, and J. Hu, Phys. Rev. Lett. **101**, 206404 (2008).
[19] V. Cvetkovic and Z. Tesanovic, Europhys. Lett. **85**, 37002 (2009).
[20] D. A. Tompsett and G. G. Lonzarich, arXiv:0902.4859.
[21] N. Colonna, G. Profeta, A. Continenza, and S. Massidda, Phys. Rev. B **83**, 094529 (2011)
[22] S. E. Sebastian, J. Gillett, N. Harrison, P. H. C. Lau, D. J. Singh, C. H. Mielke, and G. G. Lonzarich, J. Phys. Condens. Matter **20**, 422203 (2008).
[23] N. Harrison, R. D. McDonald, C. H. Mielke, E. D. Bauer, F. Ronning, and J. D. Thompson, J. Phys. Condens. Matter **21**, 322202 (2009).
[24] C. Liu *et al.*, Phys. Rev. Lett. **102**, 167004 (2009).
[25] T. Kondo *et al.*, Phys. Rev. B **81**, 060507(R) (2010).
[26] F. Chen, Y. Zhang, J. Wei, B. Zhou, L. Yang, F. Wu, G. Wu, X. H. Chen, and D. L. Feng, J. Phys. Chem. Solids **72**, 469 (2011).
[27] Y.-Z. Zhang, H. C. Kandpal, I. Opahle, H. O. Jeschke, and R. Valenti, Phys. Rev. B **80**, 094530 (2009)
[28] M. Tomic, R. Valenti, and H. O. Jeschke, Phys. Rev. B **85**, 094105 (2012)
[29] T. Yildirim, Phys. Rev. Lett. **102**, 037003 (2009).
[30] B. Saparov, C. Cantoni, M. Pan, T. C. Hogan, W. Ratcliff II, S. D. Wilson, K. Fritsch, B. D. Gaulin, and A. S. Sefat, Sci. Rep. **4**, 4120 (2014).
[31] Y. S. Oh, K. H. Kim, P. A. Sharma, N. Harrison, H. Amitsuka, and J. A. Mydosh, Phys. Rev. Lett. **98**, 016401 (2007).
[32] L. Taillefer, J. Phys. Condens. Matter **21**, 164212 (2009).
[33] F. Laliberte *et al.*, Nat. Commun. **2**, 432 (2011).
[34] N. Doiron-Leyraud *et al.*, Phys. Rev. X **3**, 021019 (2013).
[35] C. Liu *et al.*, Nat. Phys. **6**, 419 (2010).
[36] S. Arsenijevic, H. Hodovanets, R. Gaal, L. Forro, S. L. Budko, and P. C. Canfield, Phys. Rev. B **87**, 224508 (2013).
[37] M. Matusiak, Z. Bukowski, and J. Karpinski, Phys. Rev. B **81**, 020510(R) (2010).
[38] Y. Suezaki and H. Mori, Prog. Theor. Phys. **41**, 1177 (1969).
[39] See Supplemental Material at http://link.aps.org/supplemental/10.1103/PhysRevLett.112.186401 for a discussion of select transport and structural properties and the model used.
[40] J. Qi *et al.* Phys. Rev. Lett. **111**, 057402 (2013).
[41] L. Ortenzi, E. Cappelluti, L. Benfatto, and L. Pietronero, Phys. Rev. Lett. **103**, 046404 (2009).
[42] F. Ma, Z.-Y. Lu, T. Xiang, Front. Phys. China **5**, 150 (2010).
[43] F. Chen, Y. Zhang, J. Wei, B. Zhou, L. Yang, F. Wu, G. Wu, X. H. Chen, and D. L. Feng, J. Phys. Chem. Solids **72**, 469 (2011).
[44] R. S. Dhaka, R. Jiang, S. Ran, S. L. Bud'ko, P. C. Canfield, B. N. Harmon, A. Kaminski, M. Tomić, R. Valentí, and Y. Lee, Phys. Rev. B **89**, 020511R 2014).